1   Impact of upstream moisture structure on a back-building convective precipitation

2   system in south-eastern France during HyMeX IOP13

4   Keun-Ok Lee[1], Cyrille Flamant[2], Fanny Duffourg[3], Véronique Ducrocq[3], and Jean-Pierre

5   Chaboureau[1]

7   [1]Laboratoire d'Aérologie, Université de Toulouse, CNRS, UPS, Toulouse, France

8   [2]LATMOS/IPSL, CNRS, Sorbonne Université and Université Paris-Saclay, Paris, France

9   [3]CNRM, UMR 3589, Université de Toulouse, Météo-France & CNRS, Toulouse, France

11   ABSTRACT

12   The present study examines the impact of the environmental moisture structure in the lower troposphere

13   (below 2 km above sea level, ASL) on the precipitation development, observed in southern France during

14   intensive observation period 13 of the first Special Observation Period of the Hydrological cycle in the

15   Mediterranean Experiment (HyMeX SOP-1), through a series of sensitivity experiments using the non-

16   hydrostatic numerical model Meso-NH. The control simulation (CNTL) and all the other 12 sensitivity

17   experiments examined in this study succeed in reproducing a heavy precipitation event (HPE) in the coastal

18   mountainous region of Var in south-eastern France as observed. The sensitivity experiments are designed to

19   investigate the response of the variability of the water vapour content upstream in the moist marine

20   atmospheric boundary layer (MABL) and the drier air above on the HPE. The comparisons between CNTL

21   and the 12 sensitivity experiments show how the life cycle of precipitation associated with the HPE, but also

22   the upstream flow (over the sea), is modified, even for moisture contents changes of only 1 g kg^{-1} below 2

23   km ASL. Within the low-level wind convergence between southerlies and south-westerlies, a small increase

24   of moisture content in the MABL prolongs moderate precipitation ($\geq$ 5 mm in 15 min) and enlarges the area

25   of weak precipitation ($\geq$ 1 mm in 15 min). The moistening in the 1−2 km ASL layer, just above the MABL,

26   prolongs the duration of moderate precipitation, for a similar total precipitation amount as in CNTL. The

27   drier MABL and 1−2 km ASL layer shorten both the life-time of precipitation and the total precipitation

28   amount with respect to CNTL. We also found that the moisture in the MABL has a stronger impact on

1   producing enhanced precipitation (both in terms of amount and intensity) than the moisture just above (1−2

2   km ASL). Also it is worth noting that adding moisture in the MABL does not necessarily lead to enhanced

3   precipitation amount. At the same time, the duration of moderate precipitation increases with increasing

4   moisture as does the area covered by weak precipitations, while the area covered by the intense precipitation

5   (≥ 30 mm) decreases. Despite a simplified moisture-profile modification approach, this study suggests that

6   moisture structure in lower troposphere is a key for accurate prediction at short-term range of the timing and

7   location of precipitation in the coastal mountainous region in southern France.

9   ***Running title***: *Impact of upstream moisture structure on HPE*

11   **1. Introduction**

12   Most of the Mediterranean countries face heavy precipitation events (HPEs), especially during autumn. More

13   than 100 mm of precipitation in less than 6 hours is not uncommon in these regions, and such rainfall

14   accumulations often cause flash-floods with large material damages and important human losses. These high-

15   impact events are most often due to quasi-stationary Mesoscale Convective System (MCS) (*e.g.* Barthlott

16   and Davolio, 2015; Nuissier et al. 2008; Romero et al. 2000; Trapero et al. 2013a, 2013b).

17   During the autumn, the warm Mediterranean is a significant source of moistening and heating for the

18   marine atmospheric boundary layer (MABL) through latent and sensible heat fluxes (Duffourg and Ducrocq,

19   2011). The southerly low-level marine winds that prevail during HPEs over the northwestern Mediterranean

20   transport this moist and conditionally unstable air toward the coastal mountainous region (Ricard et al.

21   2011). Such low-level conditions are favoured by typical synoptic patterns. Nuissier et al. (2011) found that

22   the synoptic-scale pattern propitious to HPEs over the French Mediterranean region consist of an upper-level

23   trough located west of France and an upper-level ridge over central Europe. MCSs preferably develop

24   eastward of a slow-evolving disturbance associated with an upper-level trough and leading a south-westerly

25   diffluent flow. Such a synoptic pattern favours a persistent low-level moist and conditionally unstable marine

26   flow directed towards the costal mountainous regions.

27   When this conditionally unstable low-level flow impinges on some of the mountain range foothills that

28   border the Western Mediterranean, a back-building MCS can be triggered and renewed repeatedly at the

29   same location, as long as the same low-level and upper-level conditions persist. Orographic lifting has been

1 largely proposed in past studies as a mechanism for triggering HPEs over the western Mediterranean (*e.g.*

2 Buzzi et al. 1998; Houze, 1993; Jansa et al. 2001; Lin, 1993; Romero et al. 2015; Rotunno and Ferretti, 2001;

3 Smith, 1979; Trapero et al. 2013a, 2013b). Furthermore, other convection triggering mechanisms, stemming

4 from the low-level marine flows interaction with the complex terrain of the western Mediterranean, have

5 been highlighted (*e.g.* Ducrocq et al., 2016). The dynamical and thermodynamical characteristics of the low-

6 level flows are decisive with respect of the triggering mechanisms involved (Bresson et al. 2012).

7   The water vapour transported by the marine flow is a crucial ingredient of Mediterranean HPEs.

8 Therefore, the realistic representation of its spatio-temporal variability in numerical weather prediction

9 models is critical for HPE forecast. Predicting the initiation of convection in cloud resolving models can also

10 be highly dependent on very accurate estimates of water vapor within and just above the boundary layer (*e.g.*

11 Crook, 1996; Ducrocq et al., 2002; Weckwerth et al., 2004; Bielli et al., 2012). This requires relevant

12 moisture observations in the inflow region or within the convective storms, particularly over the sea which

13 are difficult to obtain on a regular basis in order to properly constrain numerical weather prediction models

14 in terms of moisture.

15   The first Special Observation Period (SOP-1, Ducrocq et al. 2014) of the Hydrological cycle in the

16 Mediterranean Experiment (HyMeX) took place in autumn 2012, aiming to improve our knowledge of the

17 origin and transport pattern of moist air masses in pre-convective conditions and determine the link between

18 these air masses and HPEs. During Intensive Observation Period 13 (IOP13, 14 October 2012) of HyMeX

19 SOP-1, back-building MCSs developed in south-eastern France shortly after 1300 UTC (Duffourg et al.,

20 2018). The synoptic situation of IOP13 is characterised by an upper-level trough associated with a surface

21 disturbances situated over north-western France. Ahead of the associated cold front, a south-westerly low-

22 level flow over the Mediterranean French coast brings a warm marine air mass inland. Thanks to aircraft

23 water vapour measurement acquired over the Gulf of Lion (northwestern Mediterranean) during IOP13,

24 Duffourg et al. (2018) detailed the moisture structure upstream the MCSs which was characterised by a moist

25 conditionally unstable MABL (below 1 km above sea level, ASL) topped by dry air masses just above (1−2

26 km ASL). They emphasized the importance of the low level moisture for feeding the convective systems

27 observed during this HPE and the significance of the dry air above for strengthening the associated cold

28 pools. The goal of the present study is to further investigate the impact of moist air in the boundary layer and

29 surrounding dry air masses on the development and evolution of MCSs.

1   The impact of the environmental moist structure on the development of a convective system (which

2   produced 70 mm of precipitation in 6 hours), observed a few kilometres southwest offshore of the Marseille

3   and Var coastlines in southern France, is investigated here through a series of sensitivity experiments using

4   the French non-hydrostatic numerical research model Meso-NH (Lac et al., 2018) at the horizontal grid of

5   2.5-km. The article is organized as follows: Section 2 describes the experimental design, the results of the

6   control and sensitivity simulations are presented in sections 3 and 4, and then summarised in section 5 with

7   concluding remarks.

9   **2. Numerical simulation**

10   *2.1. Meso-NH model configuration*

11   Meso-NH (Lac et al. 2018) has already shown its capability to simulate HPEs in both real and idealized

12   frameworks (Ricard, 2005; Argence et al., 2008; Nuissier et al., 2008; Ducrocq et al., 2008; Clark and

13   Chaboureau, 2010; Bresson et al., 2012). For this study, the same set-up as in Duffourg et al. (2016 and

14   2018), that proved to be able to reproduce realistic convective systems, was used. It includes the same

15   simulation domain over south-eastern France and the north-western Mediterranean (Fig. 1, 200-km × 200-km

16   domain encompassing the precipitating systems and their marine low-level moisture-supplying flow), the

17   same horizontal resolution of 2.5 km, the same vertical grid with 55 stretched vertical levels (Gal-Chen and

18   Somerville, 1975) up to 20 km and the same parametrisation schemes: the bulk 1-moment mixed

19   microphysical scheme (Caniaux et al., 1994; Pinty and Jabouille, 1998) combining a three-class ice

20   parametrisation with a Kessler's scheme for the warm processes, a 1D-turbulence parametrisation based on a

21   1.5-order closure (Cuxart et al., 2000) of the turbulent kinetic energy equation with the Bougeault and

22   Lacarrere (1989) mixing length, the Pergaud et al. (2009) Eddy Diffusivity Mass Flux scheme for shallow

23   convection, the Rapid Radiation Transfer Model for radiation and the surface model SURFEX (Masson et al.

24   2013). Transport scheme for momentum variables is a WENO (weighted essentially non-oscillatory) scheme

25   (Shu and Osher, 1988) while other variables are transported with the PPM (Piecewise Parabolic Method)

26   scheme (Collela and Woodward, 1984). An open wave radiation condition (Carpenter, 1982) combined with

27   a five-grid-point relaxation flow scheme (Davies, 1976) are applied at the boundaries.

28   The control simulation (referred to as CNTL in the following) was initialized at 0900 UTC on 14

29   October 2012. As in Duffourg et al. (2018), the initial and lateral boundary conditions are provided by the 3-

1 hourly Application of Research to Operational at Mesoscale-West Mediterranean (AROME-WMED)

2 analyses (Fourrié et al., 2015). AROME-WMED is a dedicated version of the French operational convection-

3 permitting numerical prediction system Application of Research to Operations at Mesoscale (AROME, Seity

4 et al., 2011), set up specifically for the HyMeX field campaigns and covering the western Mediterranean.

6 *2.2. Control simulation validation*

7 During IOP13, convection initiation is observed around 1200 UTC, over the sea, a few kilometres offshore

8 the coast of south-eastern France. It develops into organised convective systems (not shown) in the

9 surroundings of Marseille and along the coast of the Var region (geographical positions are given in Figure

10 1). A maximum 6-hour rainfall accumulation of 67 mm is recorded over land under the convective line

11 anchored along the Var coast between 1400 UTC and 1900 UTC on 14 October 2012. The CNTL simulation

12 succeeds in reproducing heavy precipitation over south-eastern France. The CNTL simulation starts showing

13 evidence of weak precipitation (< 5 mm per 15 min) and low reflectivity (values than 30 dBZ) around 1200

14 UTC over the sea (not shown). Then 6-hour accumulative precipitation over 5 mm is simulated over the Var

15 coast at 1230 UTC (Fig. 2b). It develops preferably toward the inland of Marseille, then around the Argens

16 valley region and the east coastal Var region (Figs. 2b and 3a−b), as similarly observed. Reflectivities larger

17 than 45 dBZ are simulated in the Argens valley region and the east coastal Var region from 1400 to 1600

18 UTC (Figs. 3b−d). The simulated amount of rainfall accumulation is realistic, with 74.2 mm in 6 hours

19 associated with the convective line over the eastern Var coast (longitude 6.5°E, Figure 2a).

20   Figure 4 displays the hourly evolution simulated by CNTL of the equivalent potential temperature, θ_e,

21 at 925 hPa and virtual potential temperature, θ_v, at the first model level (about 10 m), together with the

22 horizontal wind and the vertical velocity at 500 m ASL during the period between 1300 and 1600 UTC.

23 During this period, the marine warm and moist low-level air (θ_e > 322 K) progresses north-eastwards. At

24 1300 UTC (Fig. 4a) it reaches the Var coast and convective ascents are localized along the coast on the

25 mountain sides. From 1400 UTC on (Figs. 4b−d), the cold air (θ_v < 291 K) formed by evaporative cooling

26 under the intensifying precipitation spreads out over the plains (Fig. 3b−d and 2b). At 1400 UTC very high

27 CAPE (Convective Available Potential Energy) values (i.e. in excess of of 1590 J kg^{-1}) are simulated around

28 the Var coast in CNTL, in good agreement with the CAPE of 1600 J kg^{-1} derived from radiosounding

29 measurements in Marseille at 1500 UTC (not shown). The convection develops rapidly on the leading edge

1   of the cold air channelled in the Argens valley (geophysical positions are given in Figure 1) (Fig. 3c), then it

2   propagates to the eastern Var coast after 1600 UTC (Fig. 3d). Convection is quasi-stationary along the

3   eastern Var coastal region (Fig. 4d). The cold pool plays a major role in determining the location of the

4   precipitation (Duffourg et al., 2018).

5   To characterize the air mass supplying the precipitating system, backward trajectories of air parcels

6   reaching the top of the simulated convective ascents are performed. They show that the convective ascents

7   are fed by the south-westerly marine flow all similarly along the red dashed line drawn in Figure 1. The

8   vertical projection of the backward trajectories (not shown) provides evidence that the flow is confined to the

9   lowest 1000 m above the sea surface before being lifted up to the top of the troposphere within 1 hour in the

10   convective ascents of the precipitating system. The low-level flow brings a moist (about 10 g kg^{-1}) and warm

11   (θ_e about 322 K) air mass from the north-east of the Balearic Islands at 0900 UTC to the south-eastern

12   French coasts, where it feeds the convective ascent. Another set of backward trajectories is computed to

13   identify the air mass involved in the formation of the cold pool under the intense precipitation in the eastern

14   Var coastal region. All trajectories follow a similar pathway represented by a blue dashed line in Figure 1.

15   Moreover, the air mass involved in cold-air pool formation comes mainly from a dry layer between 1 and 2

16   km ASL, just above the moist boundary layer, with water vapour mixing ratios (WVMRs) ranging between 3

17   and 8 g kg^{-1} (not shown).

18   The water vapour contents upstream of the HPE of IOP13 (over the sea; 3.5−5.5°E, 41−42.5°N) at

19   0600 UTC on 14 October 2012 of AROME-WMED analyses data are compared with that retrieved by the

20   Special Sensor Microwave/Imager (SSM/I) at 0625 UTC of the same day. The horizontal distribution of

21   integrated water vapour (IWV) values between the AROME-WMED analyses and SSM/I are in broad

22   agreement, i.e. moister air to the north-east of Balearic Islands and drier air offshore of the south-west French

23   coast (not shown) showing a mean IWV difference of 0.7 kg m^{-2}, with averaged values of 18.2 kg m^{-2} in

24   AROME-WMED analyses Vs 18.9 kg m^{-2} in SSM/I. In AROME-WMED analyses, near 90 % of the IWV

25   concentrates below 2 km ASL, i.e. 69.5% below 1 km ASL, 21 % between 1 and 2 km ASL.

26   In the following, we will analyse the precipitating pattern and characteristics simulated over the Var

27   coastal region, and their sensitivity to the related upstream moisture environment by comparisons of results

28   between CNTL and 12 sensitivity experiments with varying water vapour content in lower troposphere

29   (below 2 km ASL).

2.3. Initial conditions of sensitivity experiments

To study the sensitivity of IOP13 precipitation to the moisture structure in the low troposphere, two sets of experiments, in which the initial WVMR profiles are modified in the moist MABL (below 1 km ASL) and in the dryer layer above (1−2 km ASL), are carried out, namely the MST and DRY experiments, respectively (Table 1 and Figures 1 and 5). The WVMR profiles are modified in the areas involved in the moisture supply of the precipitating system and in the cold pool formation. Then the impact on the precipitation amount and location is analysed. The location and extent of the "sensitivity bubbles" are defined based on the results of backward trajectory analyses (red and blue dashed lines in Fig. 1) done using CNTL. For the six MST experiments, the "sensitivity bubble" is located over the sea, centred about 230 km from the Marseille coastline (red-coloured cross in Fig. 1), with an ellipsoidal shape with a short axis of 80 km and a long axis of 160 km length (red ellipse in Fig. 1). Three MST experiments were designed, with WVMR values between 100 and 1000 m ASL in the "sensitivity bubble" being increased by 1, 2, and 5 $g\,kg^{-1}$ keeping the air under-saturated (Figure 5a and Table 1a): they are referred to as MST1P, MST2P and MST5P experiments, respectively, in the following. Likewise, three MST experiments were designed with WVMR values between 100 and 1000 m ASL in the "sensitivity bubble" being decreased by 1, 2, and 5 $g\,kg^{-1}$ (MST1M, MST2M and MST5M, respectively, see Figure 5a).

For the six DRY experiments (Table 1b), the "sensitivity bubble" is centred at about 150 km from the Marseille coastline (blue-coloured cross in Fig. 1), and has an ellipsoidal shape with a short axis of 60 km and a long axis of 120 km length (blue ellipse in Fig. 1). In these experiments, the WVMR values between 1000 and 2000 m ASL in the "sensitivity bubble" are increased (decreased) by 1, 2, and 5 $g\,kg^{-1}$ (Fig. 5b) keeping the minimum WVMR value to 0 $g\,kg^{-1}$, and they are referred to as DRY1P (DRY1M), DRY2P (DRY2M) and DRY5P (DRY5M) experiments, respectively. Other environmental conditions in MST and DRY experiments are the same as in CNTL.

The magnitude of the WVMR anomalies introduced in the "sensitivity bubbles" are based on recent studies which confronted the quality of the AROME-WMED analyses in the lower troposphere with WVMR profiling instruments operating over the Mediterranean, in particular using ground-based and airborne water vapour lidars (*e.g.* Chazette et al., 2016; Lee et al., 2016; 2017). Chazette et al. (2016) evidenced that the root mean square error between AROME and lidar WVMRs in the vicinity of Balearic Islands below 2 km ASL

1   range between 1 and 1.6 g kg^{-1}, while Lee et al. (2016) and Lee et al. (2017) highlighted differences as large

2   as 3−4 g kg^{-1} in the MABL upstream of MCSs over the Tyrrhenian Sea and the Balearic Sea, respectively.

3   For the present analysis, we consider several indicators, such as: 1) the maximum of the 6-hour

4   accumulated precipitation amount (RR$_{acc}$) and the sum of the 6-hour rainfall accumulation over the entire

5   simulation domain (RR$_{sum}$) from 1200 UTC on 14 October 2012 to understand the impact of WVMR

6   variability on precipitation amount, 2) the horizontal area (km^2) of 6-hour precipitation $\geq$ 1 mm (AR$_{01}$) and $\geq$

7   30 mm (AR$_{30}$) in CNTL, and its deviation (%) from those in the MST and DRY experiments, and 3) the

8   duration of precipitation ($\geq$ 5 mm) over the land (D$_{land}$), duration of precipitation $\geq$ 5 mm per 15 min (D$_{RR05}$),

9   and duration of precipitation $\geq$ 15 mm per 15 min (D$_{RR15}$) to investigate the WVMR impact on modifying the

10   precipitating location, intensity and duration. Those indicators are presented in Figures 6 and 10 for the

11   different sensitivity experiments (MST and DRY, respectively). Figures 7 and 13 displays the 6-hour rainfall

12   accumulation simulated in the MST and DRY sensitivity experiments, respectively. Figures 8 and 14 show

13   the evolution of the maximum 15-min accumulated precipitation amount (RR$_{max}$) every 15 min during 6

14   hours, highlighting the differences in time, intensity and location of the precipitation simulated in the MST

15   and DRY experiments, respectively. Note that the weak precipitation amounts (i.e. less than 5 mm per 15

16   min) are not displayed in these figures to focus on active convective system. Also note that the analysis of

17   the precipitation characteristics is conducted for 6 hours (from 1200 to 1800 UTC) when the convective

18   systems affect the inland and coastal regions. Precipitation continues over the sea after 1800 UTC in all

19   experiments, as observed. Figure 9 shows the temporal evolution of maximum CAPE in the "sensitivity

20   bubble" every 15 min from 0930 to 1445 UTC in CNTL, MST×M, and MST×P.

3. Sensitivity to moisture in the marine boundary layer (MST experiments)

3.1. Dried marine boundary layer

24   Decreasing the moisture contents in the MABL (0.1−1 km ASL) in MST2M and MST5M leads to less

25   precipitation with both RR$_{acc}$ and RR$_{sum}$ decreasing from 62.8 m in CNTL to 60.4 m, 56.4 m and 45.1 m in

26   MST1M, MST2M, and MST5M respectively for RR$_{sum}$ (grey bars in Fig. 6a), and from 74.2 mm in CNTL to

27   65.1 mm and 63.2 mm in MST2M and MST5M respectively for RR$_{acc}$ (white bars), while the precipitation

28   accumulation remains similar in MST1M with 75.7 mm. The duration of precipitation and their horizontal

1   extent are also reduced in MST×M experiments. The duration of intense precipitation ($\geq$ 15 mm in 15 min,

2   red dots in Fig. 8b and c; D_{RR15}, black bar in Fig. 6c) are shortened by a factor of 1.5 and 2.5 in MST2M and

3   MST5M, respectively, compared to CNTL (90 min and 45 min, instead of 120 min). Similarly, the

4   precipitating time $\geq$ 5 mm (D_{RR05}, grey bar in Fig. 6c) is shortened in MST1M and MST2M by one hour and

5   half compared to CNTL (435 min, Fig. 6c).

6   The horizontal distribution of the 6-hour accumulated precipitation simulated in MST×M experiments

7   is displayed in Figures 7a−c. It confirms that the precipitation accumulation is reduced, especially for the

8   largest amounts along the eastern coastal Var region. Approximately 25 mm less precipitation is simulated

9   along the eastern coast of Var in MST1M than in CNTL (area enclosed in solid line, Fig. 7a). In MST2M and

10   MST5M, 6-hour accumulation precipitation along the eastern coastal region remains mainly lower than 35

11   mm, whereas larger accumulations are simulated in mountainous region. Figure 6b shows that the area with

12   RR_{acc} in excess of 30 mm (AR_{30}, grey bars) is reduced by 4.4%, 35.0%, and 65.7% in MST1M, MST2M, and

13   MST5M, respectively, when compared to CNTL, whereas the deviation of area affected by the weak

14   precipitation, RR_{acc} in excess of 1 mm (AR_{01}, white bars) is reduced only by 2.8%, 3.7%, and 1.7 % in

15   MST1M, MST2M, and MST5M, respectively.

16   The temporal evolution of the location and amounts of RR_{max} (displayed in Figure 8a−c) shows that, in

17   the MST×M experiments, precipitation (RR_{max} in excess of 5 mm) starts at the same time and location as in

18   CNTL (at 1230 UTC) to the south-western coast of Var. It then shifts towards Marseille and later to the

19   eastern coastal region of Var. In MST2M and MST5M (Fig. 8b−c), the largest 15-min rainfall accumulations

20   stays longer in the mountainous region of close to Marseille (west of 6°E) than in CNTL (Fig. 2b).

21   To understand the reduction of the precipitation amount (RR_{acc} and RR_{sum}) and of the precipitating

22   duration along the eastern Var coast, Figure 9 shows the CAPE values upstream the precipitation in CNTL

23   (solid line) and MST×M (dashed lines) from 0930 UTC to 1445 UTC. At 1000 UTC, the CAPE is reduced

24   by about 35, 67, and 95 % in MST1M, MST2M, and MST5M, respectively, compared to CNTL (1083 J kg^{-}

25   ^{1}). In MST1M, MST2M, and MST5M, CAPE values increase gradually until 1445 UTC but remain lower

26   than CNTL. At 1400 UTC, the spatial distribution of the decreased CAPE values ($\leq$ 1000 J kg^{-1}) is

27   highlighted offshore of the Var coast (5.2−6°E, 42.4−43°N, dashed ellipsoid in Figure 10b) in MST2M,

28   where higher CAPE values (>1400 J kg^{-1}) are displayed in CNTL (Figure 10a). Figure 11a−c shows that the

29   warm equivalent potential temperature of the air mass over the Mediterranean and the coastal region ($\theta_e >$

1   322 K at 925 hPa) is reduced in MST×M at 1500 UTC in comparison to CNTL (Fig. 4c). The cold air mass

2   (θ_v < 291 K at the first model level) formed along the foothill of mountain by evaporation of the intense

3   precipitation is also weakened in MST×M (Figure 11a−c). Moreover in MST2M and MST5M (Figure

4   11b−c), the cold pool weakened further with the weakened vertical wind at the southern edge of the cold

5   pool. This combination of decreased CAPE and weakened cold pool can explain the weakened precipitation

6   (Figs. 7a−c) especially around the Argens valley region (Figs. 8a−c). After 1600 UTC, the cold air mass (θ_v <

7   291 K) intensifies along the eastern Var coastal region showing the intensified vertical wind at its southern

8   edge (not shown) and the location of RR_{max} (red dots, ≥ 15 mm) shifts to the north-eastern Var coast (Fig.

9   8a−c).

10   In summary, a decrease in moisture in the MABL results in a reduction of the precipitation amount

11   intensity, and in a shortening of the precipitation duration. The reduction of precipitation is highlighted both

12   around the Argens valley region and over the eastern coast of the Var region because the lifted air is too dry

13   to reach condensation along the coast on the mountainsides with reduced CAPE values, while larger

14   precipitation remains in the mountainous region by the continuous supplies of low-level moist air as CNTL.

16   *3.2. Moistened marine boundary layer*

17   Figure 6 does not show significant differences between MST1P and CNTL except for an increase of RR_{acc}

18   (from 74.2 mm in CNTL to 83mm in MST1P) and a decrease of D_{land} (from 315 min in CNTL to 240 min in

19   MST1P). In MST2P, and MST5P experiments, the increase of the moisture content in the MABL (0.1−1 km

20   ASL) induces more precipitation over the sea than in CNTL. The D_{RR05} (grey bar in Figure 6f) is increased

21   significantly with 480 min, and 660 min in MST2P and MST5P instead of CNTL of 435 min, while D_{land}

22   (white bar) is reduced to 270 min, and 180 min in MST2P, and MST5P, respectively instead of 315 min in

23   CNTL. Besides, the horizontal area covered by precipitation in excess of 1 mm (AR_{01}, white bar in Figure

24   6e) which is enlarged by 17.4% and 26.0% in MST2P, and MST5P, respectively, while AR_{30} (grey bar) is

25   reduced by 30.5% and 51.5%, respectively. This indicates more widespread but weaker precipitation in

26   MST2P and MST5P simulations. For MST2P, RR_{sum} is not significantly modified while RR_{acc} increases to

27   81.8 mm, more than 74.2 mm in CNTL, and for MST5P, RR_{sum} decreases from 62.8 m in CNTL to 56.4 m,

28   while RR_{acc} decreases.

29   The 6-hour accumulated precipitation in MST1P experiments displayed in Figure 7d confirms that in

1   the MST1P, the largest accumulation on the eastern Var coast is increased (consistently with the increase of

2   RR_{acc}, Fig. 6d) and slightly shifted offshore (consistently with the reduced D_{land}, Fig. 6f) (area enclosed by

3   solid line, Fig. 7d). The temporal evolution of the location and amounts of the maximum of 15-min

4   accumulated rainfall (Figure 8d) shows that this accumulation is due to a stationary system blocked over the

5   Var coast, similarly as in CNTL. The precipitating system is blocked by a cold air pool ($\theta_v < 291$ K) over the

6   Argens valley as shown by Figure 11d.

7   For MST2P, Figure 7e still shows a large accumulation on the eastern Var coast due to a stationary

8   system blocked by a cold air pool (Figure 11e) but also an increase of weak precipitation over the sea

9   consistently with Figure 6 results. The precipitation pattern in MST5P shown by Figures 7f and 8f is quite

10   different from that in CNTL, with more widespread precipitation over the sea (around 6°E, 42°N) and with

11   much less precipitation (64 mm) along the eastern coast of Var (east of 6°E).

12   The large accumulation of precipitation on the eastern Var coast and the increase of weak precipitation

13   over the sea in MST1P and MST2P can be explained by the consistently high CAPE values upstream the

14   precipitation area from 0930 UTC to 1445 UTC compared to CNTL (Figure 9). With the high CAPE values,

15   Figures 8d−f also show that precipitation in MST×P simulations starts earlier over the sea than in CNTL

16   (Figure 2b) (consistently with the increased D_{RR05}). At 1000 UTC, 1 and 2 g kg^{-1} increase in moisture in the

17   MABL increases upstream CAPE values by 29 and 55.5 % in MST1P and MST2P, respectively, compared to

18   CNTL (1083 J kg^{-1}). At 1400 UTC (Figure 10c), the high CAPE (≥ 1300 J kg^{-1}) in MST2P is seen offshore

19   of the Var coast (6°E, 42.5°N, dashed ellipsoid in Figure 10c). Figure 11d−e shows that the marine air mass

20   advected towards the coast is warmer and moister ($\theta_e > 324$ K) in MST1P and MST2P than in CNTL (Fig.

21   4a−b).

22   The widespread and weaker precipitation over the sea particularly seen in MST5P is associated to a

23   less organized precipitating system when the moisture content in the MABL is increased. Regarding the less

24   organized system in MST5P, the absence of a cold pool is highlighted (Figure 11f) while CAPE values

25   higher than 1500 J kg^{-1} consistently favours the upstream environment triggering the precipitation over the

26   sea (blue solid line in Figure 9).

27   In summary, increasing the WVMR in the MABL enables an earlier initiation of convection over the

28   sea. Within the warm and moist air mass advected towards the Var region, a small increase of moisture

29   content in MABL favours convection triggering. Precipitation is weaker, more scattered and widespread for a

1   WVMR increase exceeding 2 g kg^{-1} in MABL. This precipitation pattern was similarly seen in an

2   environment of very moist boundary layer of Bresson et al. (2012).

4   ***4. Sensitivity to moisture between 1 and 2 km ASL (DRY experiments)***

6   *4.1. Dried lower troposphere between 1 and 2 km ASL*

7   Decreasing moisture contents in the dry layer at 1−2 km ASL in DRY1M, DRY2M, and DRY5M reduces the

8   total accumulated precipitation in the whole simulation domain (RR$_{sum}$ equal to 61.9 m, 59.6 m, and 57.5 m,

9   respectively, instead of 62.8 mm in CNTL, Figure 12a). However the total amount of precipitation simulated

10   in the DRY×M experiments remains larger than for MST×M experiments with a drier MABL (e.g. RR$_{sum}$

11   equal to 60.4 m, 56.4 m and 45.1 m for MST1M, MST2M, and MST5M, respectively). This indicates that

12   the precipitation amount is more sensitive to the moist air in the MABL (below 1 km ASL) than the air just

13   above (1−2 km ASL). The duration of precipitation (D$_{RR05}$ and D$_{land}$) are also reduced (Fig. 12c). The area

14   affected by precipitation (AR$_{01}$) is reduced as well, especially for accumulation ≥ 30 mm (AR$_{30}$) and for a

15   change of WVMR larger than 2 g kg^{-1} (Fig. 12b). However, the precipitation accumulation (RR$_{acc}$) is slightly

16   increased in DRY1M and DRY2M (80.7 mm and 81.7 mm respectively), and remains similar to CNTL (74.2

17   mm) in DRY5M (73.7 mm).

18   The horizontal distributions of the 6-hour accumulated precipitation in DRY×M experiments are

19   displayed in Figure 13a−c. The maximum of precipitation located along the eastern Var coast (closed circle)

20   is about 15−20 mm smaller than in CNTL. The temporal evolution of the location and amounts of the

21   maximum of 15-min accumulated rainfall every 15 min in DRY×M experiments is displayed in Fig. 14a−c.

22   In DRY×M experiments, RR$_{max}$ ≥ 5 mm starts about at the same time (or slightly later) than in CNTL.

23   However, precipitation is initiated at a more realistic location, closer to Marseille (about 5.5°E), especially in

24   DRY2M and DRY5M, instead of the southern tip of the Var region (about 6°E) of CNTL (Figure 2b).

25   Figure 15a−c displays the hourly evolution simulated by DRY×M simulations of θ_e at 925 hPa and θ_v

26   at the first model level (about 10 m high), together with the horizontal wind and the vertical velocity at 500

27   m ASL at 1500 UTC. It shows a weaker cold pool with higher θ_v values (~1.5 K) along the east coastal

28   region of Var (6.2−7.2°E) in DRY×M simulations (Fig. 15a−c), compared to CNTL (Fig. 4c). The ascents

29   (green areas) at the southern edge of the cold pool (θ_v ≤ 291 K) are consistently slightly reduced in DRY1M,

1   DRY2M, and DRY5M, compared to CNTL. This is consistent with the reduction of the rainfall accumulation

2   over the Var coast in DRY×M simulations. Modifying the moisture content in the dry layer at 1−2 km ASL

3   does not change much the CAPE values upstream the precipitation (not shown). The CAPE values in both

4   CNTL and DRY×M slightly increased over the time from 1083 to 1650 J kg^{-1} in the location of the

5   "sensitivity bubble" (not shown).

6   In summary, decreasing the moisture content in the dry layer between 1 and 2 km ASL reduces the

7   total amount of precipitation as well as the area affected by the precipitation and the duration of the

8   precipitating episode. The maximum of precipitation located along the eastern Var coast is reduced,

9   corresponding to a weakened cold pool and weakened ascents at its southern boundary.

11   *4.2. Moistened lower troposphere between 1 and 2 km ASL*

12   The experiments DRY1P, DRY2P and DRY5P with increased moisture content in lower troposphere between

13   1−2 km ASL produced a similar total precipitation accumulation (RR$_{sum}$ 63.5 m, 62.6 m and 63.4 m in Fig.

14   12d) to CNTL (62.8 mm). The duration of precipitation D$_{RR05}$ is prolonged from 435 min in CNTL to 465

15   min, 510 min, and 510 min, in DRY1P, DRY2P, and DRY5P respectively (Fig. 12f). However, the duration

16   of precipitation over land (D$_{land}$) and the duration of more intense precipitation (D$_{RR15}$, ≥ 15 mm in 15 min)

17   are shortened (from 315 min in CNTL to 270 min, 240 min, and 240 min in DRY1P, DRY2P and DRY5P,

18   respectively for D$_{land}$, and from 120 min in CNTL to 105 min, 60 min and 30 min, in DRY1P, DRY2P and

19   DRY5P respectively for D$_{RR15}$). The areas of precipitation AR$_{01}$ and AR$_{30}$ are not much modified in DRY1P

20   and DRY2P simulations and both are slightly reduced in DRY5P (Fig. 12e).

21   The horizontal distribution of the 6-hour accumulated precipitation in the DRY×P experiments is

22   displayed in Figure 13d−f. The precipitation pattern is not much modified, but the maximum precipitation

23   amount over the eastern coastal region of Var is slightly shifted offshore and reduced mainly in DRY2P and

24   DRY5P (with 65.8 mm and 65.9 mm instead of 74.2 mm in CNTL, east of 6°E, Figure 13e and f).

25   The temporal evolution of the location and amount of the maximum of 15-min accumulated rainfall

26   every 15 min in DRY×P experiments (Fig. 14d−f) shows that increasing the moisture contents in the dry

27   layer between 1 km and 2 km ASL induces an initiation of the precipitation about 1 hour earlier than in

28   CNTL (consistently with the increase of D$_{RR05}$). The precipitation starts at 1200 UTC about 50 km offshore

29   the southern Var coast with larger 15-min accumulation values (10−20 mm, black and red dots in Fig. 14e−f,

compared to grey dots < 10 mm in CNTL in Fig. 2b). Regarding the large precipitation around the southern

Var coast in DRY2P and DRY5P, Figure 15e−f shows the large affected area by the cold pool (θ_v < 291 K)

compared to CNTL (Fig. 4a) at 1500 UTC. In DRY1P, DRY2P and DRY5P, the duration of the entire episode

is increased, but the intensity of the precipitation is reduced (red dots in Fig. 14d−f; D_{RR15} decreases in Fig.

12f). It also appears that the precipitation is less stationary.

In summary, increasing the moisture content in the dry lower troposphere between 1 and 2 km ASL

enlarges the precipitating area, particularly over the sea, but with weakened precipitation intensity and less

stationary system.

5. Summary

The present study examines the impact of the environmental moisture structure of the lower troposphere

(below 2 km ASL) on the precipitation development and organisation, observed in southern France during

IOP13 of the HyMeX SOP-1, through a series of sensitivity experiments using the non-hydrostatic numerical

model Meso-NH. The moisture structure upstream of the IOP13 HPE is characterised by a moist

conditionally unstable MABL (below 1 km ASL) topped by dry air mass just above (1-2 km ASL). A CNTL

simulation shows that the moisture supply to the precipitating system is provided by the moist air mass of the

MABL, while the dry air mass between 1 and 2 km ASL is involved in the formation of a cold pool.

Focusing on these two layers, namely (1) a moist layer from 0.1 to 1 km ASL, and (2) a dry layer from 1 to 2

km ASL, 12 sensitivity experiments were carried out to study the influence of upstream moisture structure in

the lower troposphere on convection development occurred in southern France.

The control simulation (CNTL), as well as all the other sensitivity experiments examined in this study,

succeed in reproducing heavy precipitation in the coastal mountainous region of Var in south-eastern France.

Through comparisons between CNTL and the 12 sensitivity experiments, we show how the life cycle of

precipitation is modified even for moisture contents changes as small as 1 g kg^{-1} below 2 km ASL. The

results are summarized schematically in Figure 16. Increasing the moisture content by 1, 2 or 5 g kg^{-1} in the

MABL (0.1−1 km ASL) (see Fig. 16a) induces an earlier initiation of precipitation offshore of the Var region

(light blue area) with an increase of CAPE values, as well as longer lasting precipitations. A small increase of

moisture content in the warm and moist MABL favours convection triggering. In the environment with an

increase of the MABL moisture content lower than 2 g kg^{-1}, precipitation developing offshore arrives to the

1   coastal region of Var with the low-level south-westerlies warm and moist air and anchors over the coasts as it

2   is blocked by a cold pool (blue line). For an increase of the moisture content exceeding 2 g kg^{-1}, the area of

3   intense precipitation around the coastal region is reduced and the precipitating system is less stationary

4   because of a weakened cold pool.

5   Similarly, moistening the layer at 1−2 km ASL (see Fig. 16c), just above the MABL, produces

6   precipitation earlier offshore (light blue area), but does not increase the total amount of precipitation nor

7   upstream CAPE values. Precipitation lasts longer and affects a larger area, particularly over the sea, but with

8   weakened precipitation intensity (dark blue area) and less stationarity (blue line).

9   A drier MABL (Fig. 16b) shortens the life-time of precipitation and reduces the total precipitation

10   amount. For instance, a 2 g kg^{-1} decreased moisture content in the MABL results in a reduction of about

11   10 % in terms of total precipitation in the coastal regions of Var (closed area with blue broken line), and in a

12   reduction of about 67 % in term of CAPE. A drier lower troposphere in the 1−2 km ASL layer (see Fig. 16d)

13   also contributes to reduce the precipitating area (light blue area) with rainfall accumulation located more

14   inland rather than over the coastal region because of a weakened cold pool. Decreasing the moisture content

15   in MABL has a stronger impact on precipitation both in terms of amount and intensity than decreasing the

16   moisture content in the layer just above (1−2 km ASL).

17   Despite a simplified moisture profile modification approach, this study suggests that moisture

18   structure in lower troposphere (below 2 km ASL) is a key for an accurate prediction of the timing and

19   location of precipitation in the coastal mountainous region (e.g. the Var region) in southern France. At the

20   same time, this study shows the importance of accurate moisture content (amount and profile) in the initial

21   field to reproduce realistic convective systems, emphasizing the importance of high-resolution and three-

22   dimensional moisture observation upstream the HPE, especially over the sea. This study focused on the

23   impact of moisture contents on precipitation development in southern France, and the HPE which occurred

24   during IOP13 of the HyMeX SOP-1. It would be interesting to consider other regions in the Mediterranean

25   basin by analysing additional HPE cases of SOP-1 when interesting moisture structure including the

26   presence of dry air masses above 2 km ASL upstream of the HPE were identified, e.g., IOP13 in south Italy

27   (Lee et al., 2016) and IOP8 in north-east of Iberian plateau (Bouin et al., 2017).

Acknowledgements

This work was supported by the French Agence Nationale de la Recherche (ANR) via the IODA-MED Grant ANR-11-BS56-0005, the MUSIC grant ANR-14-CE01-014 and the MISTRALS/HyMeX programme. This work was partly supported by DRIHM.

References

Argence, S., Lambert, D., Richard, E., Chaboureau, J.P., and Söhne, N.: Impact of initial condition uncertainties on the predictability of heavy rainfall in the Mediterranean: a case study. Q. J. R. Meteorol. Soc, 134, 1775−1788, doi: 10.1002/qj.314, 2008.

Barthlott, C. and Davolio, S.: Mechanisms initiating heavy precipitation over Italy during the HyMeX Special Observation Period 1: A numerical case study using two mesoscale models. Q. J. R. Meteorol. Soc, doi: 10.1002/qj.2630, 2015.

Bougeault, P. and Lacarrère, P.: Parameterization of orography-induced turbulence in a meso-beta-scale model. Mon. Weather Rev. 117(8): 1872−1890, 1989.

Bouin, M. N., Redelsperger, J. L., and Leveaupin, B. C.: Processes leading to deep convection and sensitivity to sea-state representation during HyMeX IOP8 heavy precipitation event. Q. J. R. Meteorol. Soc, doi: 10.1002/qj.3111, 2017.

Bresson, E., Ducrocq, V., Nuissier, O., Ricard, D., and de Saint-Aubin C.: Idealized numerical simulations of quasi-stationary convective systems over the Northwestern Mediterranean complex terrain. Q. J. R. Meteorol. Soc. 138:1751−1763, doi: 10.1002/qj.1911, 2012.

Buzzi, A., Tartaglione, N., and Malguzzi, P.: Numerical simulations of the 1994 Piemont flood: Role of the orography and moist processes. Mon. Weather Rev. 126: 2369−2383, 1998.

Carpenter K.: Note on the paper: Radiational condition for the lateral boundaries of limited-area numerical models by MJ Miller and AJ Thorpe. Q. J. R. Meteorol. Soc. 108:717−719, 1982.

Caniaux, G., Redelsperger, J. L., and Lafore, J. P.: A numerical study of the stratiform region of a fast-moving squall line. J. Atmos. Sci. 51(14): 2046−2074, 1994.

Clark, H. and Chaboureau, J.P.: Uncertainties in short-term forecasts of Mediterranean heavy precipitation event: Assessment with satellite observations. J. Geophys. Res., 115, D22213, 2010.

1   Chazette, P., Flamant, C., Raut, J. C., Totems, J., and Shang, X.: Tropical moisture enriched storm tracks

2   over the Mediterranean and their link with intense rainfall in the Cevennes-Vivarais area during

3   HyMeX. Q. J. R. Meteorol. Soc. 142: 320−334, doi:10.1002/qj.2674, 2016.

4   Collela, P. and Woodward, P. R.: The piecewise parabolic method (PPM) for gas dynamical simulations. J.

5   Comput. Phys. 54: 174−201, doi:10.1016/0021-9991(84)90143-8, 1984.

6   Crook, N. A.: Sensitivity of moist convection forced by boundary layer processes to low-level

7   thermodynamic fields. Mon. Wea. Rev., 124, 1767−1785, 1996.

8   Cuxart, J., Bougeault, P., and Redelsperger, J. L.: A turbulence scheme allowing for mesoscale and large-

9   eddy simulations. Q. J. R. Meteorol. Soc. 126(562): 1−30, doi: 10.1002/qj.49712656202, 2000.

10   Davies, H.: A lateral boundary formulation for multi-level prediction models. Q. J. R. Meteorol. Soc.

11   102:405−418, 1976.

12   Ducrocq, V., Braud, I., Davolio, S., Ferretti, R., Flamant, C., Jansa, A., Kalthoff, N., Richard, E., Taupier-

13   Letage, I., Ayral, P.A., Belamari, S., Berne, A., Borga, M., Boudevillain, B., Bock, O., Boichard, J. L.,

14   Bouin, M. N., Bousquet, O., Bouvier, C., Chiggiato, J., Ciimini, D., Corsmeier, U., Coppola, L.,

15   Cocquerez, P., Defer, E., Delanoë, J., Di Girolamo, P., Doerenbecher, A., Drobinski, P., Dufournet, Y.,

16   Fourrié, N., Gourley, J.J., Labatut, L., Lambert, D., Le Coz, J., Marzano, F.S., Molinié, G., Montani,

17   A., Nord, G., Nuret, M., Ramage, K., Rison, W., Roussot, O., Said, F., Schwarzenboeck, A., Testor, P.,

18   Van Baelen, J., Vincendon, B., Aran, M., and Tamayo, J.: HyMeX-SOP1: The Field Campaign

19   Dedicated to Heavy Precipitation and Flash Flooding in the Northwestern Mediterranean. Bull. Am.

20   Meteorol. Soc. 95: 1083−1100, doi:10.1175/BAMS-D-12-00244.1, 2014.

21   Ducrocq, V., Davolio, S., Ferretti, R., Flamant, C., Santaner, V. H., Kalthoff, N., Richard, E., and Wernli, H.:

22   Introduction to the HyMeX Special Issue on 'Advances in understanding and forecasting of heavy

23   precipitation in the Mediterranean through the HyMeX SOP1 field campaign'. Q. J. R. Meteorol. Soc.

24   142, Issue S1, 1−6, 2016.

25   Ducrocq, V., Nuissier, O., Ricard, D., Lebeaupin, C., and Thouvenin, R.: A numerical study of three

26   catastrophic precipitating events over southern France. II: Mesoscale triggering and stationarity

27   factors. Q. J. R. Meteorol. Soc. 134: 131−145, 2008.

28   Ducrocq, V., Ricard, D., Lafore, J. P., and Orain, F.: Storm-scale numerical rainfall prediction for five

29   precipitating events over France: On the importance of the initial humidity field. Weather and

1   Forecasting 17: 1236−1256, 2002.

2   Duffourg, F. and Ducrocq, V.: Origin of the moisture feeding the heavy precipitating systems over

3   southeastern France. Nat. Hazards Earth Syst. Sci. 11: 1163−1178, 2011.

4   Duffourg, F., Lee, K. O., Ducrocq, V., Flamant, C., Chazette, P., and Di Girolamo, P.: Role of moisture

5   patterns in the backbuilding formation of HyMeX IOP13 Heavy Precipitating Systems. Q. J. R.

6   Meteorol. Soc. 144: 291−303, doi:10.1002/qj.3201, 2018.

7   Duffourg, F., Nuissier, O., Ducrocq, V., Flamant, C., Chazette, P., Delanoë, J., Doerenbecher, A., Fourrié,

8   N., Di Girolamo, P., Lac, C., Legain, D., Martinet, M., Saïd, F., and Bock, O.: Offshore deep

9   convection initiation and maintenance during the HyMeX IOP 16a Heavy Precipitation Event. Q. J. R.

10   Meteorol. Soc. 142 (S1): 259−274, doi:10.1002/qj.2725, 2016.

11   Fourrié, N., Bresson, E., Nuret, M., Jany, C., Brousseau, P., Doerenbecher, A., Kreitz, M., Nuissier, O.,

12   Sevault, E., Bénichou, H., Amodei, M., and Pouponneau, F.: Arome-wmed, a real-time mesoscale

13   model designed for the HyMeX special observation periods. Geosci. Model Dev. 8(2): 1801−1856,

14   doi:10.5194:/gmdd-8-1801-2015, 2015.

15   Gal-Chen, T. and Somerville, R. C. J.: On the use of a coordinate transformation for the solution of the

16   Navier-Stokes equations. J. Comput. Phys. 17: 209−228, doi:10.1016/0021-9991(75)90037-6, 1975.

17   Houze, R. J.: Cloud Dynamics, International Geophysics Vol. 53. Academic Press: New York, NY, 1993.

18   Jansa, A., Genoves, A., Picornell, M. A., Campins, J., Riosalido, R., and Carretero, O.: Western

19   Mediterranean cyclones and heavy rain. Part 2: Statistical approach. Meteorol. Appl. 8: 43−56,

20   doi:10.1017/ S1350482701001049, 2001.

21   Lac, C., Chaboureau, J. P., Masson, V., Pinty, J. P., Tulet, P., Escobar, J., Leriche, M., Barthe, C., Aouizerats,

22   B., Augros, C., Aumond, P., Auguste, F., Bechtold, P., Berthet, S., Bieilli, S., Bosseur, F., Caumont,

23   O., Cohard, J. M., Colin, J., Couvreux, F., Cuxart, J., Delautier, J., Dauhut, T., Ducrocq, V., Filippi,

24   J.B., Gazen, D., Geoffroy, O., Gheusi, F., Honnert, R., Lafore, J. P., Lebeaupin, Brossier C., Libois,

25   Q., Lunet, T., Mari, C., Maric, T., Mascart, P., Mogé, M., Molinié, G., Nuissier, O., Pantillon, F.,

26   Peyrillé, P., Pergaud, J., Perraud, E., Pianezze, J., Redelsperger, J. L., Ricard, D., Richard, E., Riette, S.,

27   Rodier, Q., Schoetter, R., Seyfried, L., Stein, J., Suhre, K., Taufour, M., Taufour, M., Thouron, O.,

28   Turner, S., Verrelle, S., Vié, B., Visentin, F., Vionnet, V., and Wautelet, P.: Overview of the Meso-NH

29   model version 5.4 and its application. Geosci. Model Dev. in discussion, 2018.

1   Lee, K. O., Flamant, C., Ducrocq, V., Duffourg, F., Fourrié, N., and Davolio, S.: Convective initiation and
2   maintenance processes of two back-building mesoscale convective systems leading to heavy
3   precipitation events in Southern Italy during HyMeX IOP 13. Q. J. R. Meteorol. Soc, 142: 2623−2635,
4   doi: 10.1002/qj.2978, 2016.

5   Lee, K. O., Flamant, C., Ducrocq, V., Duffourg, F., Fourrié, N., Delanoë, J., and Bech, J.: Initiation and
6   development of a mesoscale convective system in the Ebro River Valley and related heavy
7   precipitation over northeastern Spain during HyMeX IOP15a. Q. J. R. Meteorol. Soc, 143: 942−956,
8   doi: 10.1002/qj.2851, 2017.

9   Lin, Y.: Orographic effects on airflow and mesoscale weather systems over Taiwan. Terr. Atmos. Ocean 4:
10   381−420, 1993.

11 Masson, V., Le Moigne, P., Martin, E., Faroux, S., Alias, A., Alkama, R., Belamari, S., Bardu, A., Boone, A.,
12   Bouyssel, F., Brousseau, P., Brun, E., Calvet, J.C., Carrer, D., Decharme, B., Delire, C., Donier, S.,
13   Essaouini, K., Gibelin, A. L., Giordani, H., Habets, F., Jidane, M., Kerdraon, G., Kourzeneva, E.,
14   Lafaysse, M., Lafont, S., Lebeaupin, BC., Lemonsu, A., Mahfouf, J.F., Marguinaud, P., Mokhtari, M.,
15   Morin, S., Pigeon, G., Salgado, R., Seity, Y., Taillefer, F., Tanguy, G., Tulet, P., Vincendon, B.,
16   Vionnet, V., and Voldoire, A.: The surfex v7.2 land and ocean surface platform for coupled or offline
17   simulation of earth surface variables and fluxes. Geosci. Model Dev. 6(4): 929−960, doi:10.5194/gmd-
18   6-929-2013, 2013.

19 Nuissier, O., Ducrocq, V., Ricard, D., Lebeaupin, Brossier C., and Anquetin, S.: A numerical study of three
20   catastrophic precipitating events over southern France. I: Numerical framework and synoptic
21   ingredients. Q. J. R. Meteorol. Soc. 134: 111−130, 2008.

22 Nuissier, P., Joly, B., Joly, A., Ducrocq, V., and Arbogast, P.: A statistical downscaling to identify the large-
23   scale circulation patterns associated with heavy precipitation events over southern France. Q. J. R.
24   Meteorol. Soc. 137: 1812−1827, doi:10.1002/qj.866, 2011.

25 Pergaud, J., Masson, V., Malardel, S., and Couvreax, F.: A parameterization of dry thermals and shallow
26   cumuli for mesoscale Numerical Weather Prediction. Bound.-Lay. Meteorol. 132(1): 83−106,
27   doi:10.1007/s10546-009-9388-0, 2009.

28 Pinty, J. P. and Jabouille, P.: A mixed-phased cloud parametrization for use in a mesoscale non-hydrostatic
29   model: Simulations of a squall line and of orographic precipitation. In: Proc. Of the Conference on

1   Cloud Physics. Amer. Meteorol. Soc, Boston: Everett, WA, USA, 17−21 Aug. 1998. Pp. 217−220,

2   1998.

3   Ricard, D., Ducrocq, V., and Auger, L.: A climatology of the mesoscale environment associated with heavily

4   precipitating events over a northwestern mediterranean area. J. Appl. Meteorol. Climatol. 51:

5   468−488, doi:10.1175/JAMC-D-11-017.1, 2012.

6   Rotunno, R. and Ferretti, R.: Mechanisms of intense Alpine rainfall. J. Atmos. Sci. 58: 1732−1749, 2001.

7   Romero, R., Ramis, C., and Homar, V.: On the severe convective storm of 29th October 2013 in the Balearic

8   Islands: Observational and numerical study. Q. J. R. Meteorol. Soc, doi:10.1002/qj.2429, 2015.

9   Romero, R., Sumner, G., Ramis, C., and Genoves, A.: A classification of the atmospheric circulation patterns

10   producing significant daily rainfall in the Spanish Mediterranean area. Int. J. Climatol. 19: 765−785,

11   1999.

12 Shu, C. W. and Osher, S.: Efficient implementation of essentially non-oscillatory shock-capturing schemes.

13   Journal of Computational Physics 77(2): 439−471, 1988.

14 Smith, R.: The influence of mountains on the atmosphere. Adv. Geophys. 21: 87−230, 1979.

15 Trapero, L., Bech, J., and Lorente, J.: Numerical modelling of heavy precipitation events over Eastern

16   Pyrenees: Analysis of orographic effects. Atmos. Res. 123: 368−383, 2013a.

17 Trapero, L., Bech, J., Duffourg, F., Esteban, P., and Lorente, J.: Mesoscale numerical analysis of the

18   historical November 1982 heavy precipitation event over Andorra (Eastern Pyrenees). Nat. Hazards

19   Earth Syst. Sci. 13: 2969−2990, 2013b.

20 Weckwerth, T., Parsons, D. B., Koch, S. E., Moore, J. A., LeMone, M. A., Demoz, B. B., Flamant, C.,

21   Geerts, B., Wang, J., and Feltz, W. F.: An overview of the International H2O Project (IHOP-2002) and

22   some preliminary highlight. Bull. Am. Meteorol. Soc. 85: 253−277, 2004.

1   **Table 1.** List of sensitivity experiment and WVMR modifications with respect to the control simulation (CNTL).

(a) Exp.	MST1M	MST2M	MST5M	MST1P	MST2P	MST5P
Max WVMR difference	-1 g kg^{-1}	-2 g kg^{-1}	-5 g kg^{-1}	$+1$ g kg^{-1}	$+2$ g kg^{-1}	$+5$ g kg^{-1}
Altitudes modified			0.1 to 1 km above sea level			
(b) Exp.	DRY1M	DRY2M	DRY5M	DRY1P	DRY2P	DRY5P
Max WVMR difference	-1 g kg^{-1}	-2 g kg^{-1}	-5 g kg^{-1}	$+1$ g kg^{-1}	$+2$ g kg^{-1}	$+5$ g kg^{-1}
Altitudes modified			1 to 2 km above sea level			

3
4
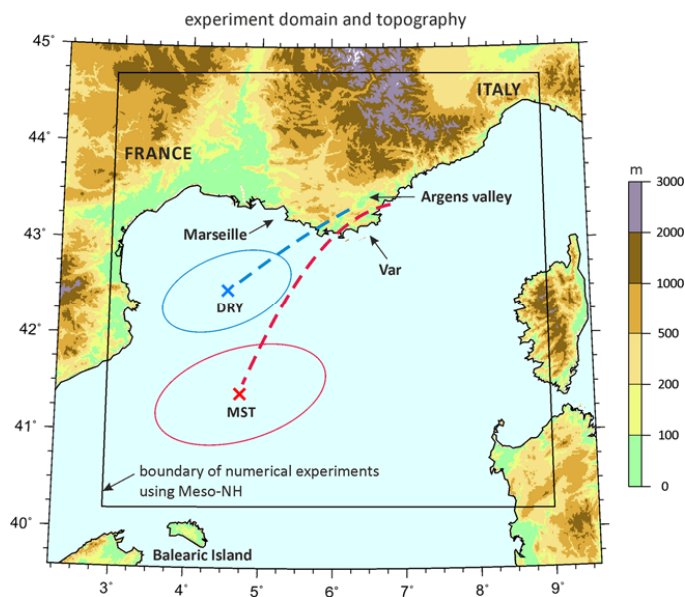
Figure 1. Topography and domain (black box) considered in numerical simulations using Meso-NH with a resolution of 2.5 km. The centre location of the initial "sensitivity bubble" set in MST and DRY experiments is depicted by red- and blue- coloured cross mark, respectively, while the horizontal range of the initial bubbles are marked by an ellipse-shaped solid line of the same colour. The red dashed line indicates the horizontal projection of backward trajectories of some air parcels taken in the upper part of the convective systems of the eastern Var coast, and the blue dashed line depicts the horizontal projection of backward trajectories of some air parcels taken in the cold pool generated by the convective systems over the eastern Var coast.
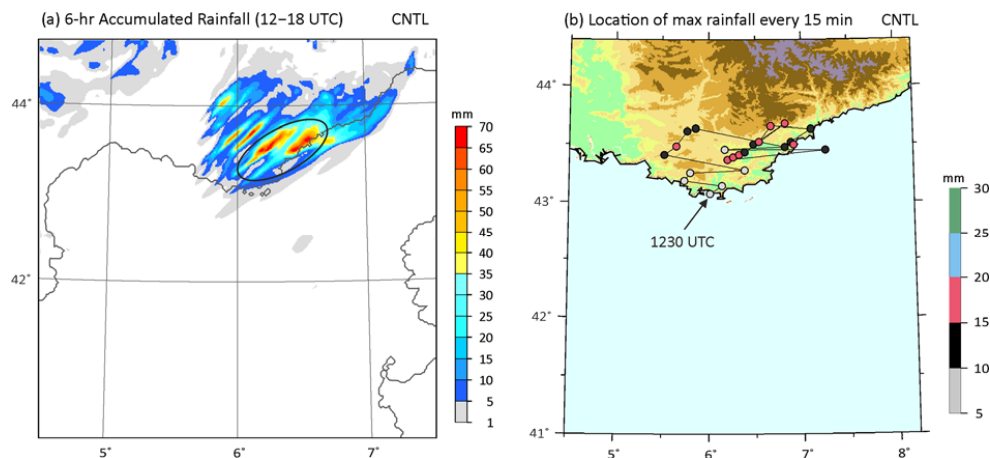
Figure 2. (a) 6-hour accumulated precipitation at 18 UTC, and (b) evolution every 15 min between 12 UTC and 18 UTC of the locations of maximum 15-min accumulated rainfall amount (RR$_{max}$) simulated by the control run (CNTL) on 14 October 2012. Also shown is the topography (see Figure 1 for the scale).
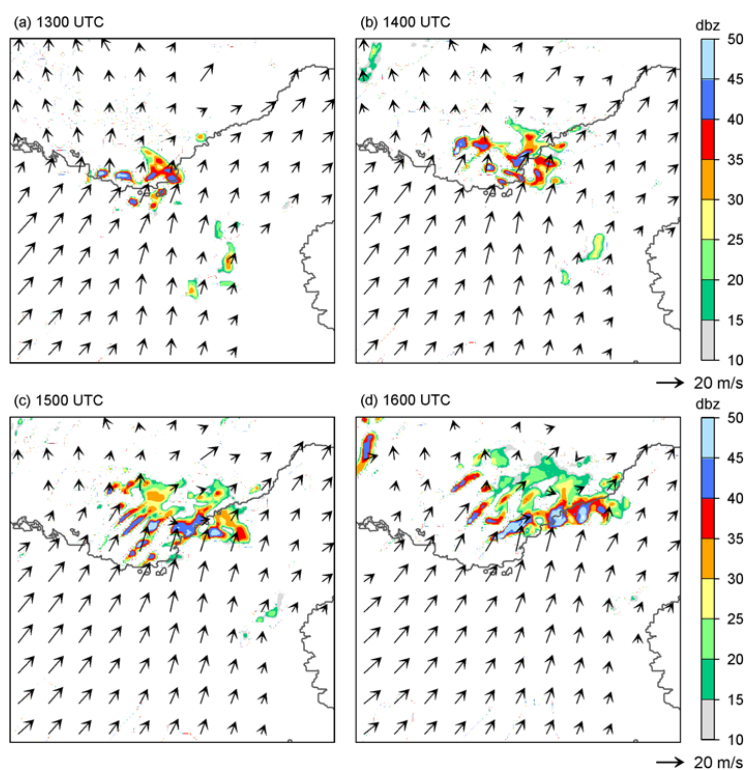
Figure 3. Radar reflectivity (dBZ) and horizontal winds simulated in CNTL at 2000 m ASL at (a) 1300 UTC, (b) 1400 UTC, (c) 1500 UTC and (d) 1600 UTC on 14 October 2012.
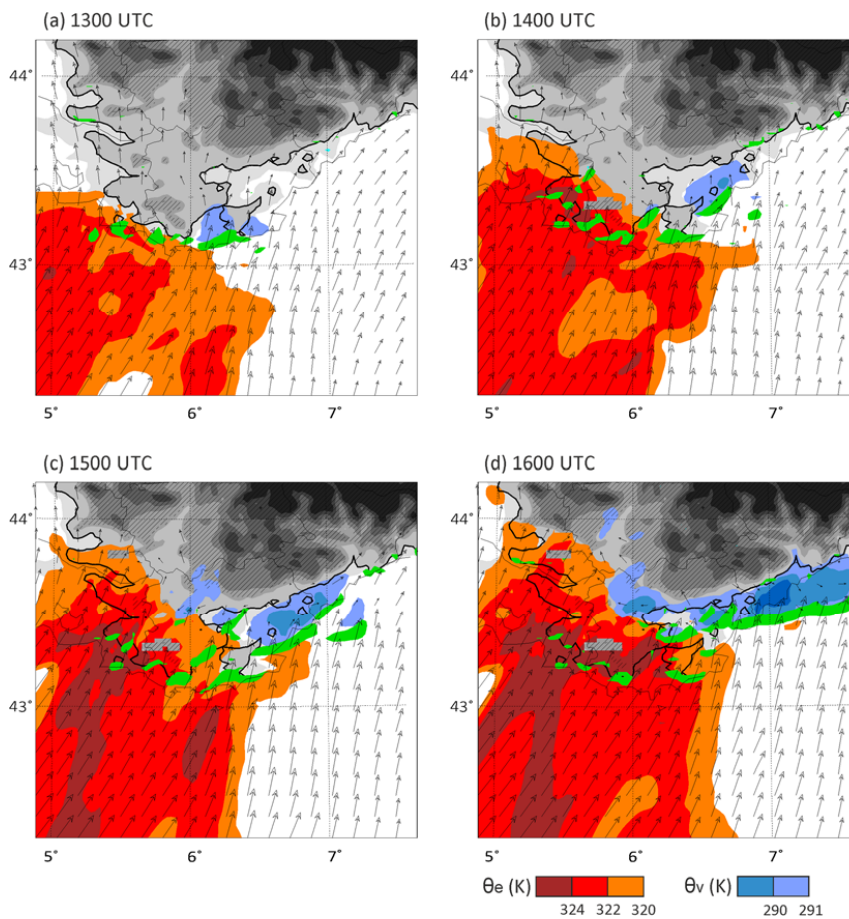
Figure 4. Equivalent potential temperature θ_e at 925 hPa (K, red areas), virtual potential temperature θ_v at the first model level (K, blue areas below 291 K), vertical wind speed at 500 m ASL (green areas above 0.5 m s^{-1}) and horizontal wind at 925 hPa (arrows) simulated by CNTL at (a) 1400 UTC, (b) 1500 UTC, (c) 1600 UTC and (d) 1700 UTC on 14 October 2012.
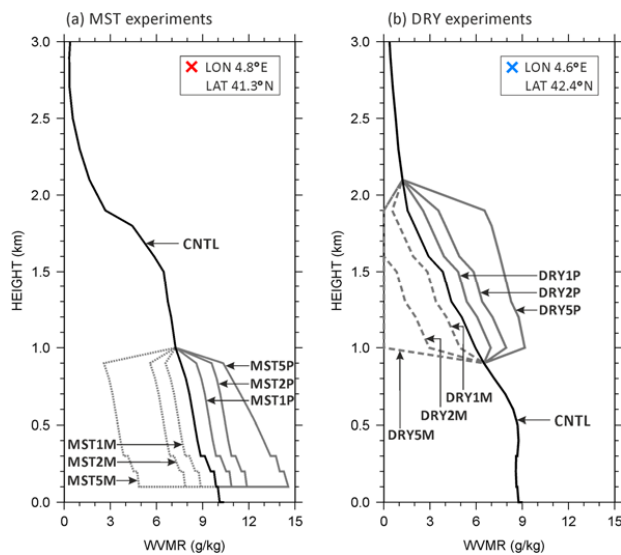
2
3 **Figure 5.** Vertical profiles of WVMR in the centre of the initial "sensitivity bubble" used in (a) MST experiments, and

4 (b) DRY experiments. Black solid lines are vertical profiles of the CNTL run at the same grid point as in MST and DRY.

5 Solid grey lines represent experiments in which WVMR was augmented, while dashed grey lines represent experiments

6 for which WVMR was reduced. The centre location of the initial "sensitivity bubble" used in MST and DRY are shown

7 in Figure 1.

9
10
11
12
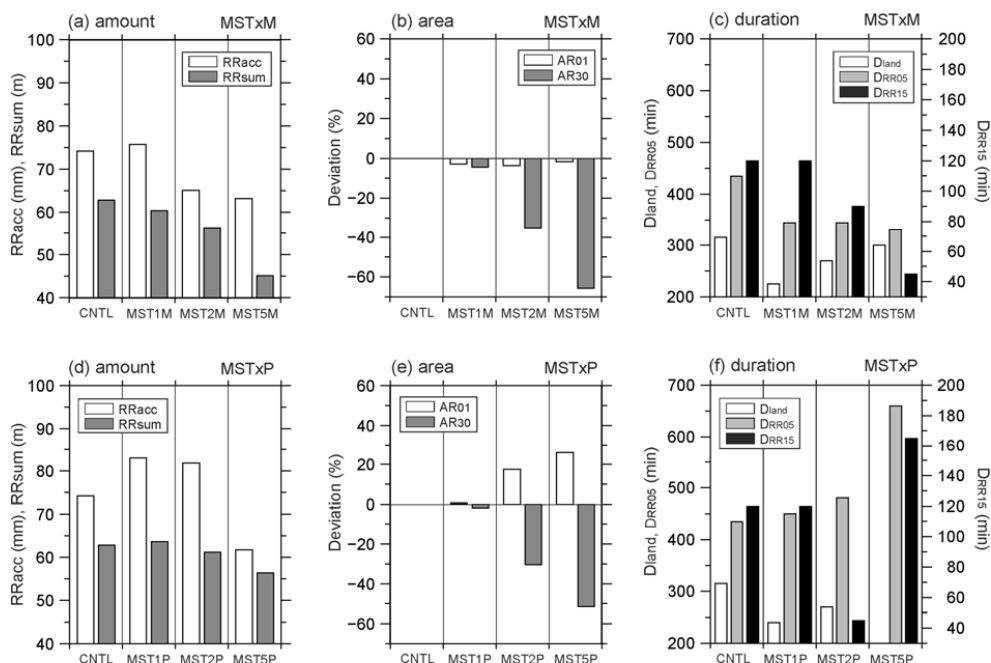
Figure 6. Results of CNTL, MST×M (upper panel, a−c) and MST×P (bottom panel, d−f) experiments: (a) and (d) 6-hour accumulated precipitation amount (RR_{acc}), and the RR_{acc} sum within the domain (RR_{sum}) from 1200 UTC on 14 October 2012, (b) and (e) the areas (km^2) of $RR_{acc} \geq 1$ mm (AR01) and $RR_{acc} \geq 30$ mm (AR30), and (c) and (f) duration of precipitation (≥ 5 mm) over the land (D_{land}), duration of precipitation $\geq$ than 5 mm per 15 min (D_{RR05}), duration of intense precipitation ≥ 15 mm per 15 min (D_{RR15}). In (b) and (e), the deviation (%) of AR01 and AR30 in MST to the ones in CNTL are displayed.
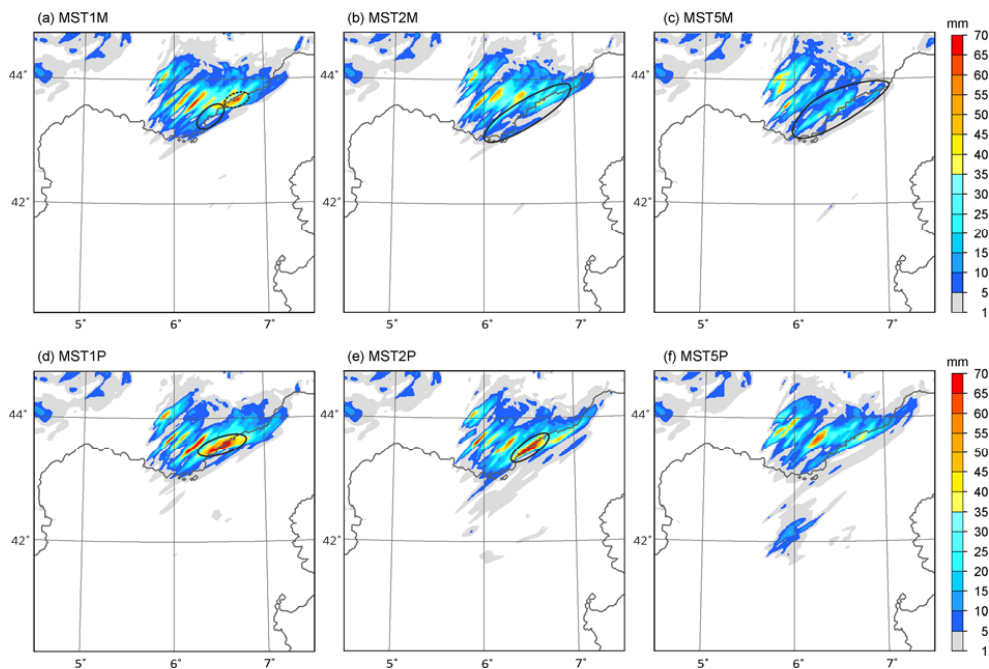
Figure 7. Distribution of the 6-hour accumulated precipitation simulated by (a) MST1M, (b) MST2M, (c) MST5M, (d) MST1P, (e) MST2P, and (f) MST5P at 18 UTC on 14 October 2012. Black contour line shows the coast of southern France.
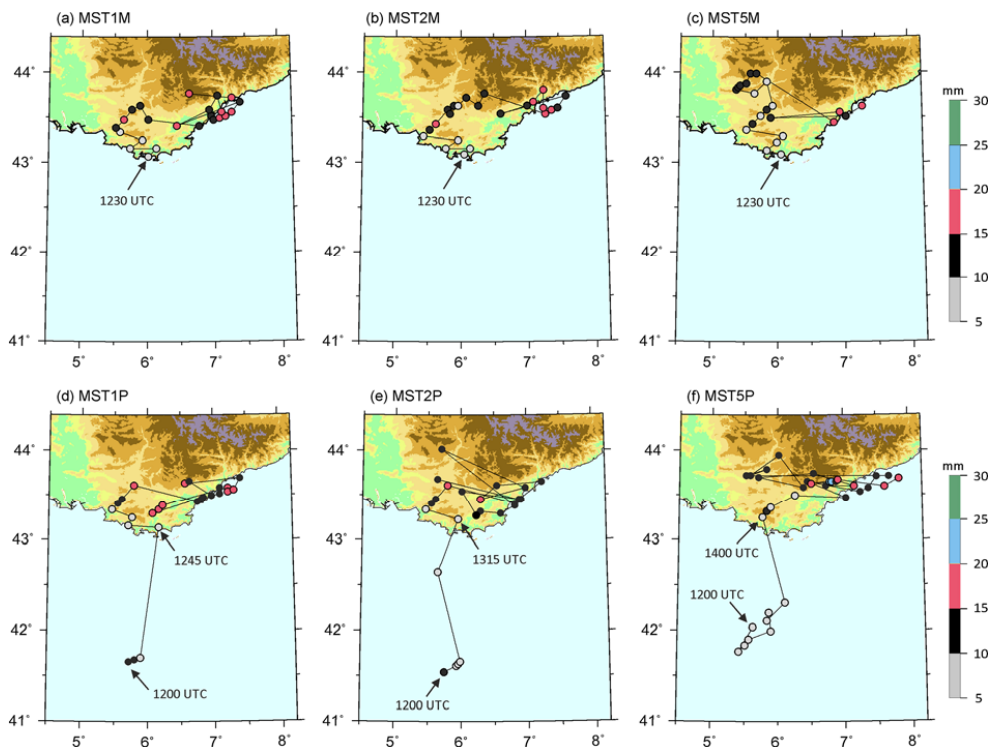
Figure 8. Evolution of the location of the maximum 15-min accumulated rainfall for 6 hours (every 15 min from 1200 UTC on 14 October 2012) simulated by (a) MST1M, (b) MST2M, (c) MST5M, (d) MST1P, (e) MST2P, and (f) MST5P. Also shown is the topography (see Figure 1 for the scale).
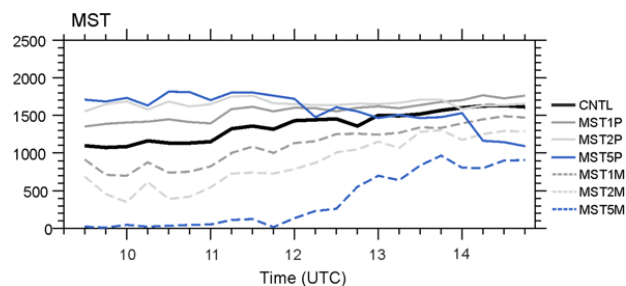
Figure 9. Temporal evolution of CAPE in the sensitivity bubble simulated by CNTL (black line), MST×P (solid lines), and MST×M (dashed line) from 0930 to 1445 UTC on 14 October 2012.
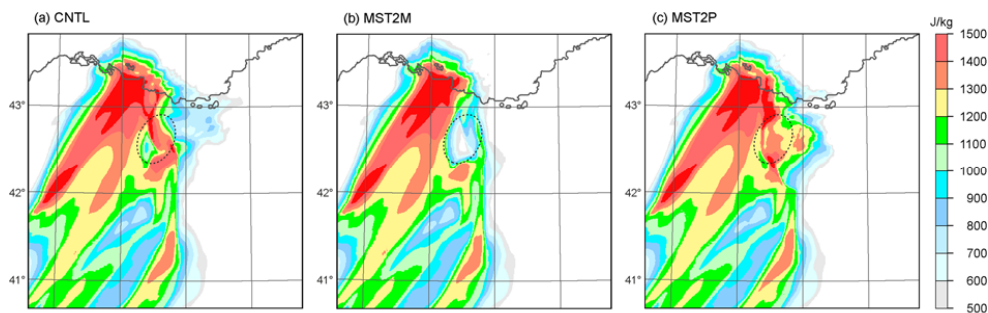
2   **Figure 10.** Distribution of CAPE simulated by (a) CNTL, (b) MST2M, and (c) MST2P at 1400 UTC on 14 October

3   2012. The dashed ellipsoid indicates location of the "sensitivity bubble".

5
6
7
8
9
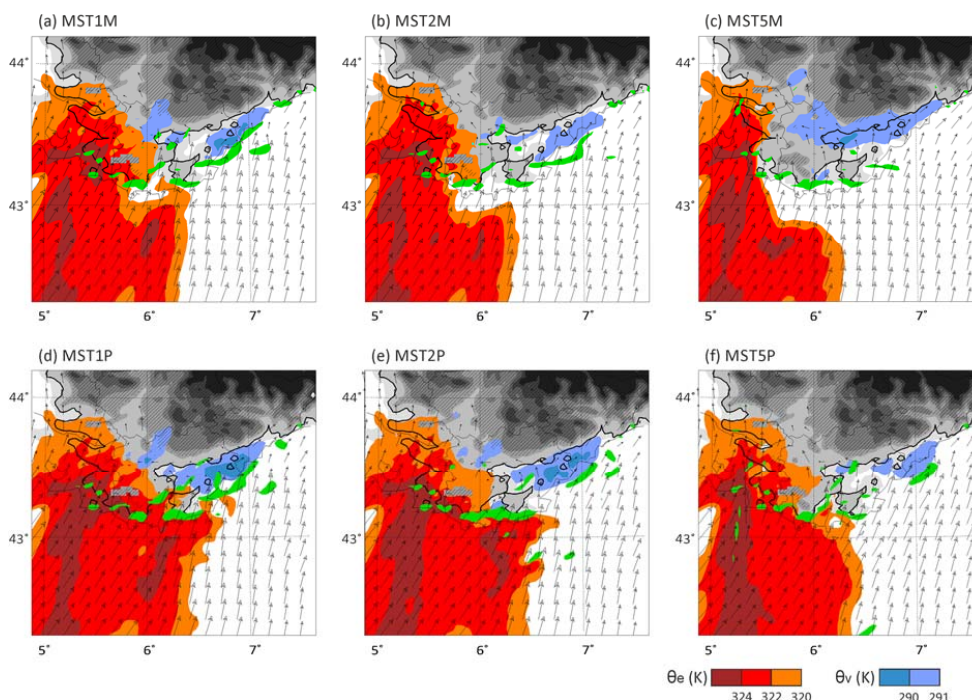
12   **Figure 11.** Equivalent potential temperature θ_e at 925 hPa (K, red areas), virtual potential temperature θ_v at the first

13   model level (K, blue areas below 292 K), vertical wind speed at 500 m ASL (green areas above 0.5 m s^{-1}, arrow) and

14   horizontal wind at 925 hPa simulated by (a) MST1M, (b) MST2M, (c) MST5M, (d) MST1P, (e) MST2P, and (f) MST5P

15   at 1500 UTC on 14 October 2012.
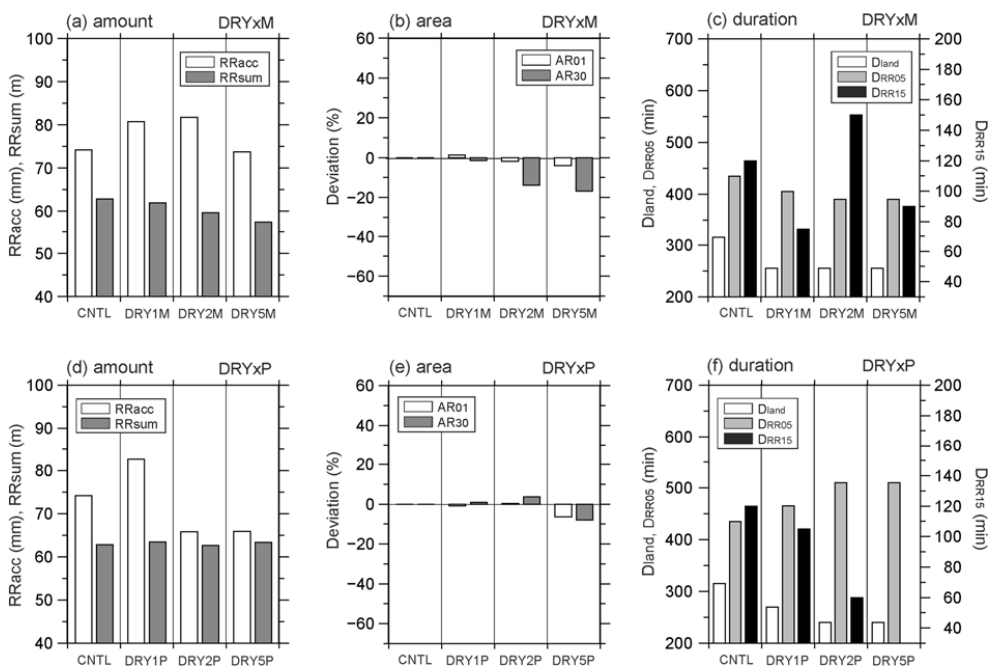
Figure 12. As Figure 6 but for CNTL, DRY×M (upper panel, a−c) and DRY×P (bottom panel, d−f) experiments.
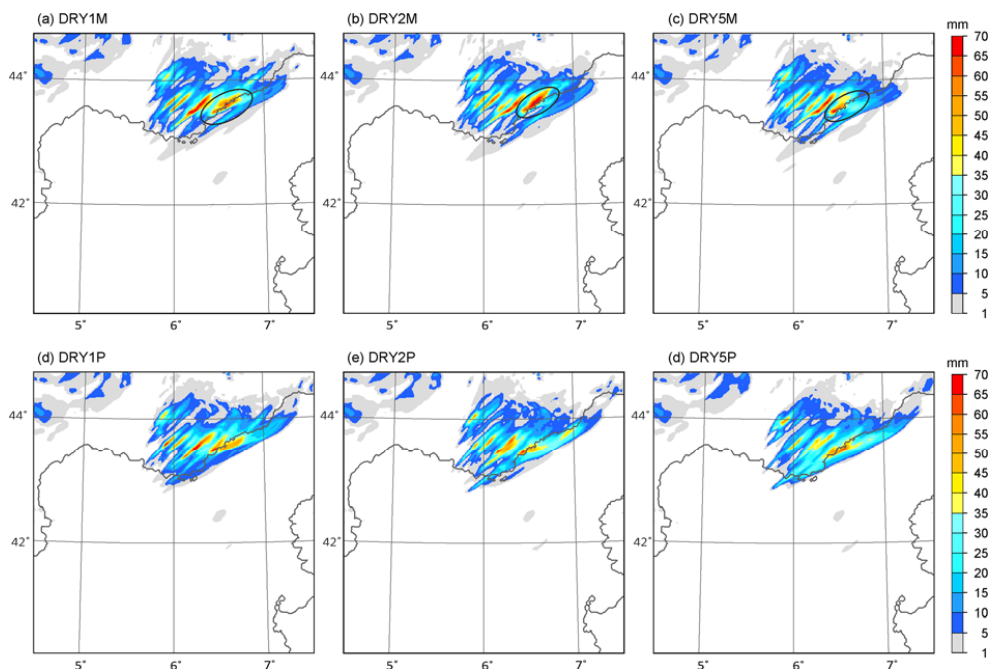
Figure 13. Same as Figure 7 for (a) DRY1M, (b) DRY2M, (c) DRY5M, (d) DRY1P, (e) DRY2P, and (f) DRY5P.
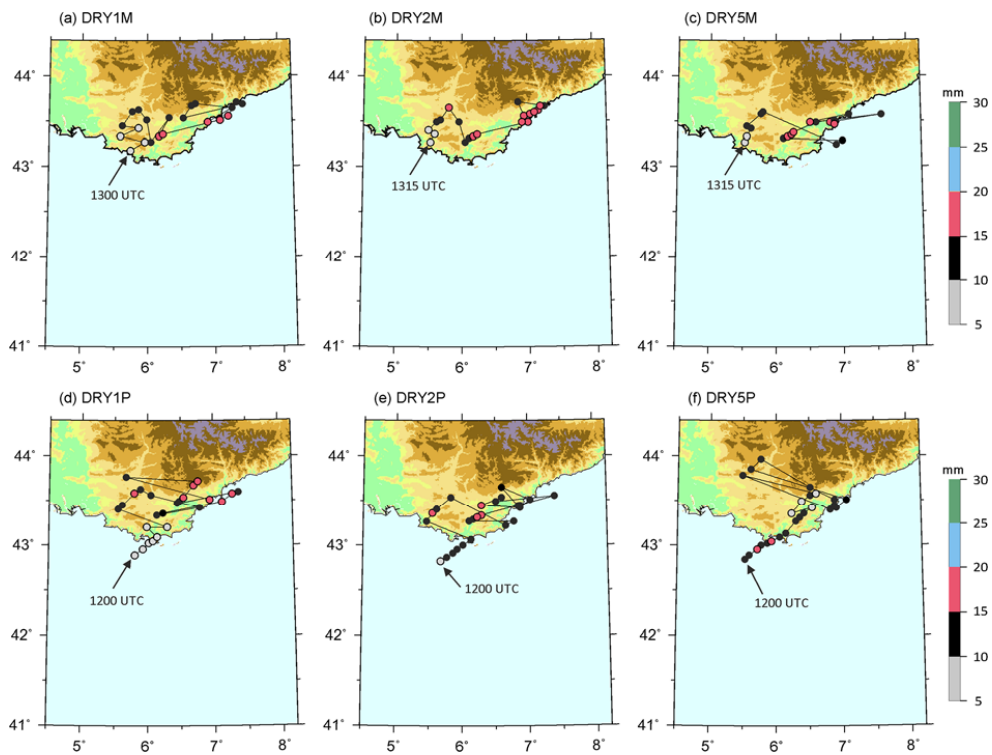
Figure 14. Same as Figure 8 for (a) DRY1M, (b) DRY2M, (c) DRY5M, (d) DRY1P, (e) DRY2P, and (f) DRY5P.
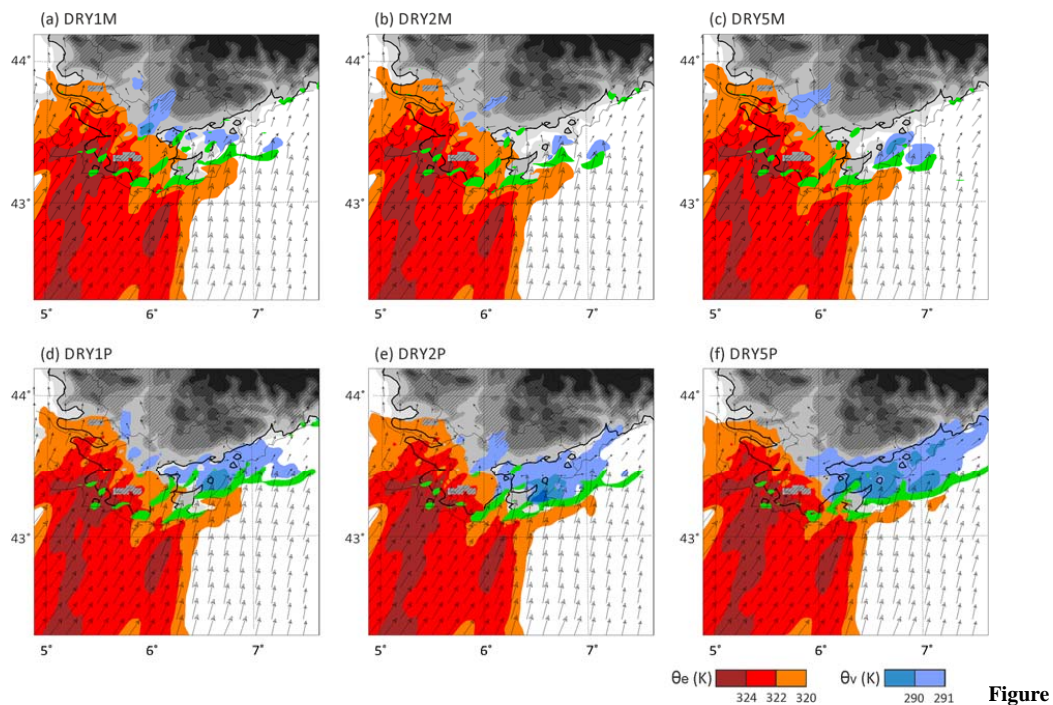
Figure

15. Same as Figure 11 for (a) DRY1M, (b) DRY2M, (c) DRY5M, (d) DRY1P, (e) DRY2P, and (f) DRY5P at 1500 UTC on 14 October 2012.
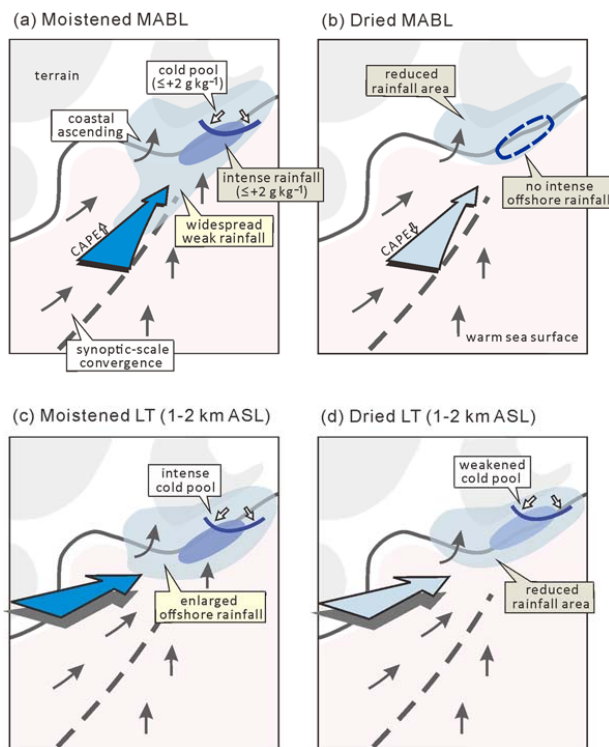
Figure 16. Schematics summarizing the main features of the impact of upstream moisture in MABL in (a) and (b), and in the lower troposphere (LT) layer between 1 and 2 km ASL in (c) and (d) on back-building heavy precipitation in south-eastern France during HyMeX IOP 13. Dark-blue arrows in (a) and (c) and light-blue arrows in (b) and (d) indicate the moistened and dried upstream air mass, respectively. In (a)−(d), black arrows and a broken line indicate the low-level wind and the synoptic-scale wind convergence line, respectively. The light-blue region depicts the weak precipitation area while the dark-blue region shows the intense precipitation area. The blue solid line illustrates the southern edge of cold pool while the closed area with blue dashed line in (b) and (d) indicates the absence of intense offshore rainfall.